1. Toufik ROUBACHE[1], 2. Souad CHAOUCH[2]

University of Msila, Algeria (1), LSP-IE Laboratory, University of Batna 2, Algeria (2)

doi:10.15199/48.2024.03.47

ANFIS Controller MPPT Algorithm for Solar powered Dual Three-Phase Induction Motor based EVs

Abstract. *In this paper, an adaptive neuro-fuzzy inference system (ANFIS) based maximum power point tracking algorithm (MPPT) are proposed for solar powered dual three phase induction motor (DTPIM) drives via input-output linearization control (IOLC). The maximum power delivery to the DTPIM is achieved by MPPT controller which employs ANFIS. It adjusts the duty cycle of the three-level boost converter for extracting maximum power from solar PV array. In addition, ANFIS is proposed for better performance of the system because has many inputs and also has multiple outputs but the fuzzy logic has multiple inputs and single output, so the combination of this two is known as ANFIS which is utilized for nonlinear applications. In order to test the performances of this control, a dynamic emulator is used. Further the propose controller is applied for electrical vehicle (EV) to determine its performance. Finally the obtained results show that the proposed controller provide a good trajectory tracking, and this scheme is robust with respect to parameter variations, and external load disturbances for DTP induction motor drive system.*

Streszczenie. *W tym artykule zaproponowano adaptacyjny algorytm śledzenia punktu mocy oparty na neurorozmytym systemie wnioskowania dla podwójnych trójfazowych silników indukcyjnych zasilanych energią słoneczną poprzez sterowanie linearyzacją wejścia i wyjścia. Maksymalne dostarczanie mocy do podwójnego trójfazowego silnika indukcyjnego jest osiągane przez kontroler śledzenia punktu maksymalnej mocy, który wykorzystuje adaptacyjny neurorozmyty system wnioskowania. Dostosowuje cykl pracy trzypoziomowej przetwornicy podwyższającej napięcie, aby uzyskać maksymalną moc z panelu fotowoltaicznego. Ponadto proponuje się adaptacyjny neurorozmyty system wnioskowania w celu lepszej wydajności systemu, ponieważ ma on wiele wejść i ma również wiele wyjść, ale logika rozmyta ma wiele wejść i jedno wyjście, więc połączenie tych dwóch jest znane jako adaptacyjne neurorozmyte wnioskowanie system stosowany w aplikacjach nieliniowych. W celu przetestowania wydajności tego sterowania używany jest dynamiczny emulator. Ponadto proponowany sterownik jest stosowany w pojeździe elektrycznym w celu określenia jego osiągów. Ostatecznie uzyskane wyniki pokazują, że proponowany sterownik zapewnia dobre śledzenie trajektorii, a ten schemat jest odporny na zmiany parametrów i zewnętrzne zakłócenia obciążenia dla dwufazowego trójfazowego układu napędowego silnika indukcyjnego. (**Algorytm MPPT sterownika ANFIS dla pojazdów elektrycznych zasilanych energią słoneczną z podwójnym trójfazowym silnikiem indukcyjnym**)*

Keywords: ANFIS, Boost Converter, Dual three phase induction motor (DTPIM), Input-output linearization control (IOLC), Electric vehicle (EV).
Słowa kluczowe: ANSW, konwerter w górę, podwójny trójfazowy silnik indukcyjny, Sterowanie linearyzacją wejścia-wyjścia, Pojazd elektryczny.

Introduction

Nowadays, solar PV is a major source of renewable energy for electricity generation in countries with high solar density. Extraction of the maximum power from the solar PV modules under various environmental circumstances, such as sun irradiance and temperature, can improve the efficiency of a solar PV system, using maximum power point tracker (MPPT). The goal of this work is to develop an ANFIS-based MPPT controller on a boost converter to enhance the performance of solar systems. The ANFIS is an information-driven method for problem solving that uses neural networks to approximate function. Typically, a preparatory set of function unknown numerical samples that need to be estimated is grouped for data-driven operations for ANFIS network synthesis [1]. Hence, the proposed scheme uses a three-level boost converter. The boosted voltage is inverted using a voltage source inverter.

According to recent studies on electrical energy consumption by electric motors, of which 90% are induction motors, consume 40% of the total amount of energy generated worldwide [2, 3]. However, the dual three phase induction motor (DTPIM) has a number of advantages, such as the capacity to handle large amounts of power without having to increase the converters' power ratings, and strong stability capabilities both at low and high speeds [4]. The DTPIM is in high power applications such as traction, like more electric aircraft, electrical and hybrid vehicles [5-9]. It is supplied by two Voltage Inverters, one is for the first stator and the second is for the second stator. The effectiveness of the proposed control system of DTPIM and estimation algorithm has been verified through simulation work at different parameter variations and torque loads. Furthermore, the control system proposed has demonstrated good performance at different robustness tests conditions. The control strategy proposed in this paper is an input-output linearization control (IOLC). Feedback linearization control can also provide a fair level of insensitivity to changes in parameters, outside disturbances, and rejection errors [10, 11].

Recently, there has been a growing demand for vehicles with ever better driving characteristics in which efficiency, safety and performance are ensured. In addition EVs are by many seen as the cars of the future as they are high efficient, produces no local pollution, are silent, and can be used for power regulation by the grid operator [12-14]. However, one of the most important applications of Photovoltaic (PV) systems is for electric vehicles (EVs) application is one of the most important areas where DTPIMs are used in order to improve vehicle performance, since these electric machines have attractive advantages in terms of low costs, less robustiveness, and higher speeds and efficiency rather than other motor/generator machines. On the other hand, solar energy is anticipated to become the world's largest source of electricity by 2050, with rapid improvements in relevant technologies and reduction in the cost of solar PV systems [14]. In this paper, we propose exploring the ANFIS concept in EV propulsion by developing an architecture applied to a doubly-fed induction motor drive fed by solar PV array. Our objective is to design a new controller to maintain the stability, robustness and tracking performance of the drive system. This paper's main contribution is the proposal of an ANFIS control approach with boost chopper for DTPIMs based on an electric vehicle. The performance of the proposed control technique in a DTPIM drive is studied for varying load operations and varying speeds.

This paper is organized as follows: In Section 2, the modeling of PV cell, DC-DC boost converter and the motor-EV are introduced. In Section 3, the adaptive neuro-fuzzy controller (ANFIS), and the IOLC associated. Simulation tests was achieved to examine the performance of a photovoltaic conversion chain intended for verify the effectiveness of the speed control under various instructions applied to the system are given in Section 4. Finally, Section 5 summarizes the conclusions of the paper.

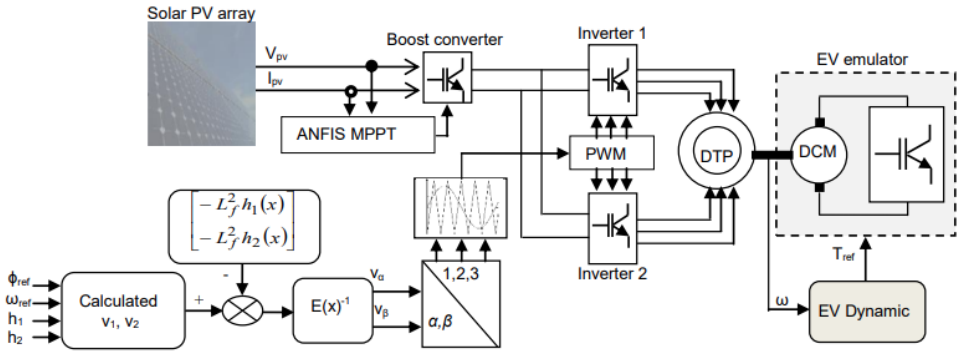

Fig.1. Block diagram of the proposed photovoltaic system powered DTPIM

System descriptions

The proposed system of the photovoltaic EV is shown in Figure 1. The schematic consists of a PV array, a three-level boost converter working as a maximum power point tracker (MPPT), two inverters and a motor driving controlled by the feedback linearization controller.

In the proposed system, solar PV array electrical output is manipulated using three-level DC–DC converter with maximum power point tracking controllers. Input for the ANFIS-MPPT controller is voltage of the solar PV panel, current of the solar PV panel, irradiance level of sun light energy, temperature of the environment and output of the MPPT controller is PWM pulse for DC–DC converter to extract maximum power from solar PV panel.

The output of the DC–DC converter is fed to voltage source PWM inverter, and output is fed to dual three phase induction motor-based electric vehicle.

PV Module

The PV module parameters are obtained from the BP 3160S PV technical datasheet (Table 1). Figure1 shows the characteristic curve of the module [15].

Table 1. The parameter values of BP 3160S PV panel

ELECTRICAL CHARACTERISTICS	BP 3160S
Optimum operation voltage	35.1 V
Optimum operation current	4.55 A
Open-circuit voltage	44.2 V
Maximum power at STC	160 W
Short-circuit current	4.8 A
Peak Efficiency	16%
Number of Cells	72
Maximum System Voltage (V for UL)	600 V
Maximum System Voltage (V for IEC)	1000 V

In order to transmit the most power to the load by adjusting the duty cycle of the boost converter, a DC-DC boost converter is designed to be placed between a solar PV module and an inverter.

DC–DC Boost converter

DC-DC converters are the power electronic circuits that convert the DC voltage to different DC voltage level and mostly produce regulated output. In this section, an integrated three-level boost converter is designed to improve the efficiency of a boost converter used in the photovoltaic application, as shown in Figure 2. This topology demonstrates higher efficiency over the conventional boost converter topology in several ways.

In a typical condition, the behavior of the circuit resembles that of the traditional design, even though it has a PV system-specific function. The total array output voltage and one of the motorized currents are used to regulate. Power switches S_1 in order to give MPPT, as suggested by the misuse of perturb and observe method.

The output voltages of the dc-link electrical devices are balanced by power switch S_2.

The working process is divided into four operating states, according to the ability switches state, which may be both conducting, each turned OFF, or one conducting and the other turned OFF.

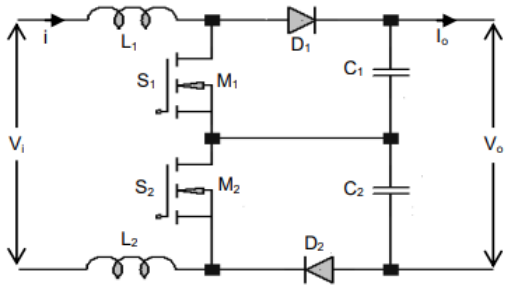

Fig.2. Block diagram three level boost converter

The equations associated with this operation mode are as follows:

$$(1)\quad \begin{cases} V_{pv1}+V_{pv2}=(L_1+L_2)\dfrac{di}{dt}+V_{c1}+V_{c2} \\ C_1\dfrac{dv}{dt}+i_o=i_{L1} \\ C_2\dfrac{dv}{dt}+i_o=i_{L2} \end{cases}$$

ANFIS control based on MPPT

The adaptive neuro-fuzzy inference is designed based on a combination of artificial neural network and fuzzy logic controller [16]. ANFIS model was trained by utilizing randomly chosen information obtained for irradiation and temperature. Irradiation level and cell temperature are inputs to the controller and its output was duty cycle.

The ANFIS algorithm was used for controlling the boost converter. This mechanism was designed to improve the performance of the drive system. Figure 3 shows the ANFIS based MPPT controller system.

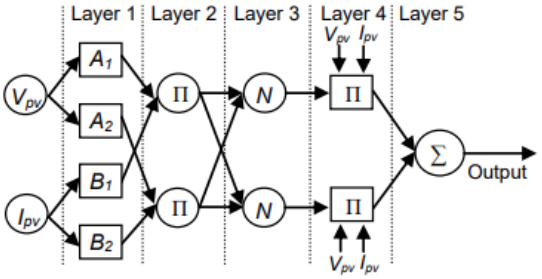

Fig.3. ANFIS typical structure

Fig.4. Training error versus epochs for the ANFIS

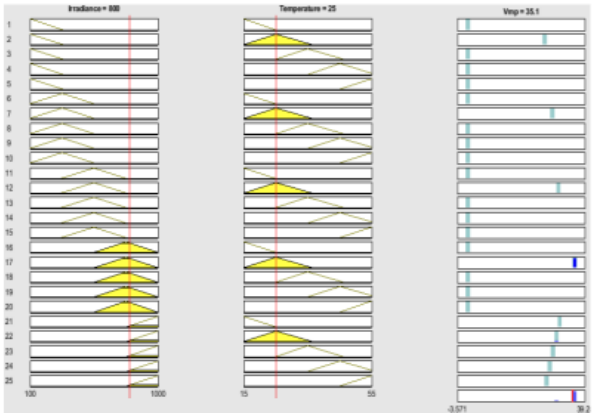

Fig.5. Rule viewer of trained FIS

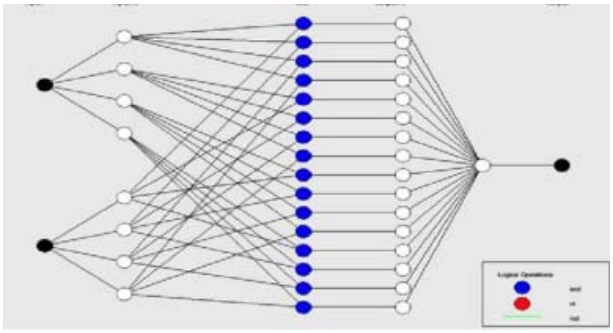

Fig.6. ANFIS model structure

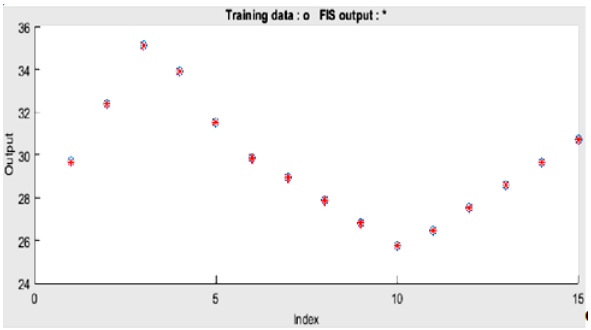

Fig.7. Final tested ANFIS system

Dual three-phase induction machine model

The modeling of the DTPIM is based on the general equations in Concordia transformation applied on the stator and rotor windings, these equations are given by [17]:

$$\dot{x}_{\alpha\beta} = Ax_{\alpha\beta} + Bu_{\alpha\beta} \tag{2}$$

Such as:

$$\begin{cases} x_{\alpha\beta} = \left[i_{s\alpha1} \quad i_{s\beta1} \quad i_{s\alpha2} \quad i_{s\beta2} \quad \varphi_{r\alpha} \quad \varphi_{r\beta} \right]^T \\ u_{\alpha\beta} = \left[u_{s\alpha1} \quad u_{s\beta1} \quad u_{s\alpha2} \quad u_{s\beta2} \right]^T \end{cases} \tag{3}$$

The mechanical part of the electrical drive is given by the following equations:

$$\begin{cases} J_t \dot{\omega} = \left(T_e - T_L - k_f \omega \right) \\ T_e = \dfrac{pL_m}{L_m + L_r} \left(\varphi_{r\alpha} i_{s\beta} - \varphi_{r\beta} i_{s\alpha} \right) \end{cases} \tag{4}$$

where J_t denotes the total inertia moment, ω is the rotor angular speed, T_e, T_L generated and load torque, respectively, k_f the friction coefficient, p the number of pairs of poles, L_m, L_r mutual and rotor inductances, respectively, $\varphi_{r\alpha\beta}$ the rotor flux, and $i_{s\alpha\beta}$ the stator current.

Assuming the mathematical model expressed by (2) and using the state variables defined by the state vector, we can define the following set of equations:

$$\begin{cases} \dot{i}_{s\alpha1} = A_1 x + b_1 u_{s\alpha1} \\ \dot{i}_{s\beta1} = A_2 x + b_1 u_{s\beta1} \\ \dot{i}_{s\alpha2} = A_3 x + b_2 u_{s\alpha2} \\ \dot{i}_{s\beta2} = A_4 x + b_2 u_{s\beta2} \\ \dot{\varphi}_{r\alpha} = A_5 x \\ \dot{\varphi}_{r\beta} = A_6 x \end{cases} \tag{5}$$

Such as:

$$\begin{cases} A_1 x = a_1 \left(- R_{s1} i_{s\alpha1} - a_2 i_{s\alpha2} - a_3 \dot{\varphi}_{r\alpha} \right) \\ A_2 x = a_1 \left(- R_{s1} i_{s\beta1} - a_2 i_{s\beta2} - a_3 \dot{\varphi}_{r\beta} \right) \\ A_3 x = a_4 \left(- R_{s2} i_{s\alpha2} - a_2 i_{s\alpha1} - a_3 \dot{\varphi}_{r\alpha} \right) \\ A_4 x = a_4 \left(- R_{s2} i_{s\beta2} - a_2 i_{s\beta1} - a_3 \dot{\varphi}_{r\beta} \right) \\ A_5 x = a_5 \left(i_{s\alpha1} + i_{s\alpha2} \right) - a_6 \varphi_{r\alpha} - a_7 \varphi_{r\beta} \\ A_6 x = a_5 \left(i_{s\beta1} + i_{s\beta2} \right) - a_6 \varphi_{r\beta} + a_7 \varphi_{r\alpha} \end{cases} \tag{6}$$

where:

$$\begin{cases} a_1 = \dfrac{1}{\sigma \left(L_m + L_s \right)}, a_2 = \dfrac{L_m L_r}{L_m + L_r}, a_3 = \dfrac{L_m}{L_m + L_r} \\ a_4 = a_1, a_5 = \dfrac{L_m}{T_r}, a_6 = \dfrac{1}{T_r}, a_7 = \omega, a_8 = \dfrac{L_m}{J_m L_r} \\ a_9 = \dfrac{-T_L}{J_m}, T_r = \dfrac{L_m + L_r}{R_r}, L_{s1} = L_{s2} = L_s, \\ b_1 = b_2 = a_1, \sigma = 1 - \dfrac{L_m^2}{\left(L_m + L_r \right)\left(L_m + L_s \right)}. \end{cases} \tag{7}$$

Vehicle dynamics

The dynamic model of an electric vehicle can be used to simulate the vehicle's performance, predict its energy consumption, and optimize its control strategy. The dynamic differential equation for the longitudinal motion of the vehicle is described using the equations [18]:

$$\begin{cases} F_t = F_a + F_r + F_p + F_s \\ J_t \dot{\omega}_w = \left(T_m - T_L \right) \\ T_L = \dfrac{T_w}{N} = \dfrac{R_w F_t}{N} \\ M_v \dot{V}_v = \left(F_L - F_t \right) \\ F_L \left(\lambda_L \right) = \mu N, \lambda_L = \dfrac{V_w - V_v}{V_v}, V_w = R_w \omega_w \end{cases} \tag{8}$$

where: F_t– total resistance force, F_a– aerodynamic drag force, F_r– rolling resistance force, F_p– profile force of the road, F_s– stokes friction force, V_v and ω_w– vehicle velocity and wheel rotational velocity respectively. T_m, T_L, T_w–driving torque, load torque, wheel torque respectively. N is transmission ratio, R_w– wheel radius, M_v– vehicle mass, F_L– road load force, μ– friction coefficient, λ_L– slip ratio.

The following equation is derived due to the use of a reduction gear.

$$\begin{cases} \omega_w = \dfrac{\omega_m}{N}, T_w = N\eta T_m \\ J_t = J_m + J_v + J_w \end{cases} \tag{9}$$

where: J_m, J_v and J_w– motor, vehicle and wheel inertia moments respectively.

Feedback linearization control of DTPIM

In this section, an input-output linearization control is applied. Firstly, we choose the outputs and inputs variables. These variables are chosen by:

$$\begin{bmatrix} z_1 \\ z_2 \end{bmatrix} = \begin{bmatrix} h_1 \\ h_2 \end{bmatrix} = \begin{bmatrix} \phi_r \\ \omega \end{bmatrix} \tag{10}$$

Such as:

(11)

$$z_1 : \begin{cases} h_1(x) = L_f h_1(x) = 2a_5 L_m f_1 - 2a_5 \phi_r \\ \ddot{h}_1(x) = L_f^2 h_1(x) + L_{G\alpha} L_f h_1(x) u_\alpha + L_{G\beta} L_f h_1(x) u_\beta \end{cases}$$

where:

$$\begin{cases} L_f^2 h_1(x) = 2a_4 a_5 L_m f_3 - 2(a_1 a_4 + 6a_4 a_5) f_1 \\ + 2a_4 a_7 f_2 + \left(\dfrac{4}{T_r} a_5 + 2a_2 a_4 \right) \phi_r \\ L_{G\alpha} L_f h_1(x) = 2a_2 L_r \varphi_{r\alpha} \\ L_{G\beta} L_f h_1(x) = 2a_2 L_r \varphi_{r\beta} \end{cases} \tag{12}$$

and:

(13)

$$z_2 : \begin{cases} h_2(x) = L_f h_2(x) = \dfrac{pL_m}{J_t L_r} f_2 - \dfrac{T_L}{J_t} \\ \ddot{h}_2(x) = L_f^2 h_2(x) + L_{G\alpha} L_f h_2(x) u_\alpha + L_{G\beta} L_f h_2(x) u_\beta \end{cases}$$

where:

$$\begin{cases} L_f^2 h_2(x) = \dfrac{pL_m}{J_t L_r} a_7 f_1 - \dfrac{pL_m}{J_t L_r} (a_1 + a_5) f_2 \\ - \dfrac{pL_m^2}{J_t L_r^2} \dfrac{a_7}{\sigma L_s} \phi_r \\ L_{G\alpha} L_f h_2(x) = -\dfrac{pL_m}{J_t L_r} b_1 \varphi_{r\beta} \\ L_{G\beta} L_f h_2(x) = \dfrac{pL_m}{J_t L_r} b_1 \varphi_{r\alpha} \end{cases} \tag{14}$$

where:

$$\begin{cases} f_1 = (i_{s\alpha 1} + i_{s\alpha 2}) \varphi_{r\alpha} + (i_{s\beta 1} + i_{s\beta 2}) \varphi_{r\beta} \\ f_2 = (i_{s\alpha 1} + i_{s\alpha 2}) \varphi_{r\beta} - (i_{s\beta 1} + i_{s\beta 2}) \varphi_{r\alpha} \\ f_3 = (i_{s\alpha 1} + i_{s\alpha 2})^2 + (i_{s\beta 1} + i_{s\beta 2})^2 \end{cases} \tag{15}$$

Although the order of the system dynamics is five, the output dynamics have an order of four, indicating the existence of an internal dynamics and the consequent stability, which could be proved with simplicity, by using input-output feedback linearization, second derivatives of the outputs are considered, and we obtain:

$$\begin{bmatrix} \ddot{h}_1 \\ \ddot{h}_2 \end{bmatrix} = \begin{bmatrix} L_f^2 h_1(x) \\ L_f^2 h_2(x) \end{bmatrix} + E(x) \begin{bmatrix} u_{s\alpha 1,2} \\ u_{s\beta 1,2} \end{bmatrix} \tag{16}$$

with:

$$\begin{cases} E(x) = \begin{bmatrix} L_{G\alpha} L_f h_1(x) & L_{G\beta} L_f h_1(x) \\ L_{G\alpha} L_f h_2(x) & L_{G\beta} L_f h_2(x) \\ -L_{G\alpha} L_f h_1(x) & -L_{G\beta} L_f h_1(x) \\ -L_{G\alpha} L_f h_2(x) & -L_{G\beta} L_f h_2(x) \end{bmatrix} \\ = \begin{bmatrix} 2a_2 L_r \varphi_{r\alpha} & 2a_2 L_r \varphi_{r\beta} \\ -\dfrac{pL_m}{J_t L_r} b_1 \varphi_{r\beta} & \dfrac{pL_m}{J_t L_r} b_1 \varphi_{r\alpha} \\ -2a_2 L_r \varphi_{r\alpha} & -2a_2 L_r \varphi_{r\beta} \\ \dfrac{pL_m}{J_t L_r} b_2 \varphi_{r\beta} & -\dfrac{pL_m}{J_t L_r} b_2 \varphi_{r\alpha} \end{bmatrix} \end{cases} \tag{17}$$

$$Det[E(x)] = 2 \frac{a_2 L_r}{\sigma L_s} \phi_r \tag{18}$$

If $(\Phi_r \neq 0)$, the matrix $E(x)$ is non-singular. By defining γ as the new control input for linear system of:

$$\gamma = \begin{bmatrix} \gamma_1 \\ \gamma_2 \end{bmatrix} = \begin{bmatrix} L_f^2 h_1(x) \\ L_f^2 h_2(x) \end{bmatrix} + E(x) \begin{bmatrix} u_\alpha \\ u_\beta \end{bmatrix} \tag{19}$$

To linearize the input-output comportments of the motor in closed loop, the main control equation can be defined as:

$$\begin{bmatrix} u_{\alpha 1,2} \\ u_{\beta 1,2} \end{bmatrix} = E(x)^{-1} \left(\begin{bmatrix} -L_f^2 h_1(x) \\ -L_f^2 h_2(x) \end{bmatrix} + \begin{bmatrix} \gamma_1 \\ \gamma_2 \end{bmatrix} \right) \tag{20}$$

As a result, the system control effort would be simplified to:

$$\gamma_1 = \ddot{h}_1 = \ddot{\phi}_r = k_{\phi 1} (\phi_{ref} - \phi_r) + k_{\phi 2} (\dot{\phi}_{ref} - \dot{\phi}_r) + \ddot{\phi}_{ref} \tag{21}$$

$$\gamma_2 = \ddot{h}_2 = \ddot{\omega} = k_{\omega 1} (\omega_{ref} - \omega) + k_{\omega 2} (\dot{\omega}_{ref} - \dot{\omega}) + \ddot{\omega}_{ref} \tag{22}$$

The gains: $k_{\Phi 1}$, $k_{\Phi 2}$, $k_{\omega 1}$ and $k_{\omega 2}$ are chosen by identification with a second order system by using the pole placement method.

Simulation results

In this section, the proposed system control input-output linearization control of DTPIM with ANFIS-MPPT based on EV emulator has been verified by simulations. The motor parameters values of the set-up are given in Table 2. The reference value of the rotor flux has been fixed to 1 wb.

Table 2. Dual three-phase induction motor parameters

Parameter	Value
Rated power	4 Kw
Stator resistance	3.72 Ω
Rotor resistance	3.72 Ω
Stator inductance	0.022 H
Rotor inductance	0.006 H
Mutual inductance	0.3672 H
Inertia moment	0.0625 kg.m^2
Friction coefficient	0.001 N.m.s/rad

The simulated results of the module under different irradiation and temperature levels are shown in Figure 8 by the current-voltage (I-V) and power-voltage (P-V) characteristics.

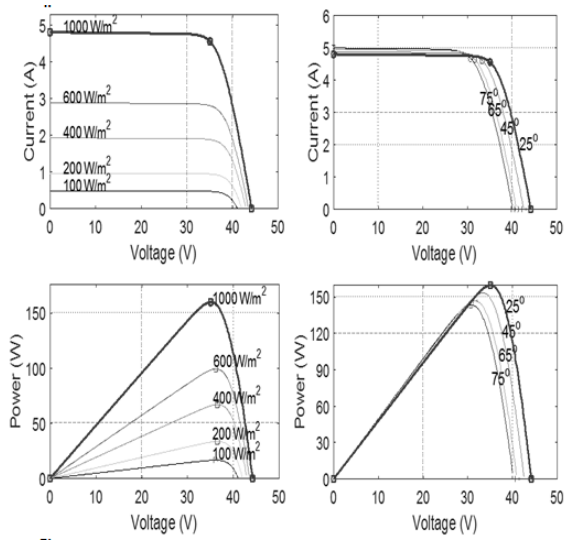

Fig.8. Simulation results of the module setup

In order to demonstrate the performance of the ANIFS-MPPT controlled boost converter PV system a number of simulations are carried out to ascertain the system performance, under both steady state and dynamic conditions.

Solar PV array is used to generate the training data set for ANFIS by varying the operating solar irradiance level in a step of 50 W/m^2 from 100 W/m^2 to 1000 W/m^2 and the temperature in steps of 5 °C from 15 °C to 55 °C.

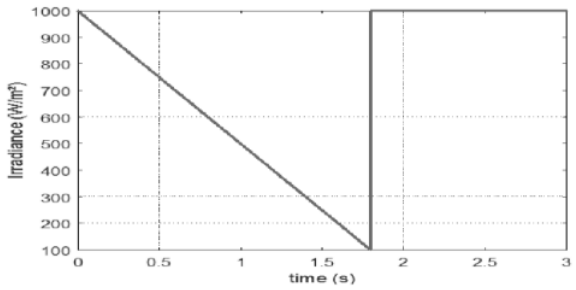

Fig.9. Irradiance plot for different values

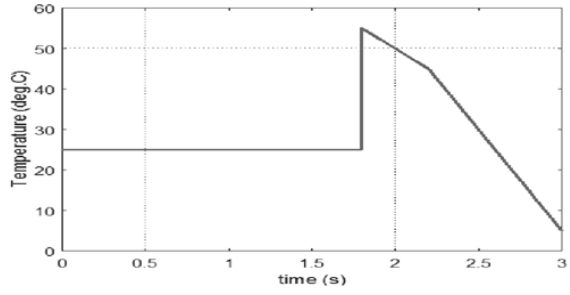

Fig.10. Temperature variation

In the simulation diagram, The PV module powers the system. The input voltage is boosted by the DC-DC converter and is fed to the three-phase voltage source inverter. The inverter determines the switching sequence and switching frequency of the DTP induction motor, essentially controlling both speed and direction of the motor. The motor is governed by IOLC, which performs speed control. The PV panel is optimized by the ANFIS-MPPT algorithm in order to extract the maximum possible energy from sunlight. The obtained results are illustred in Figure 11 and Figure 12.

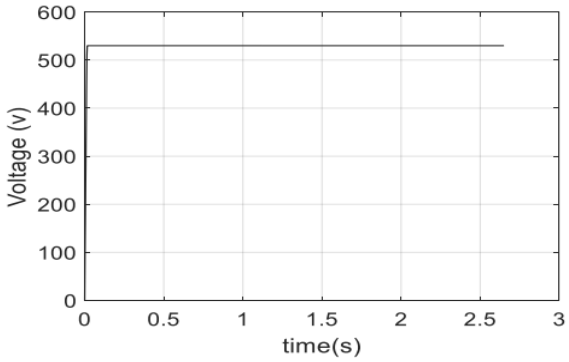

Fig.11. Output voltage of boost converte

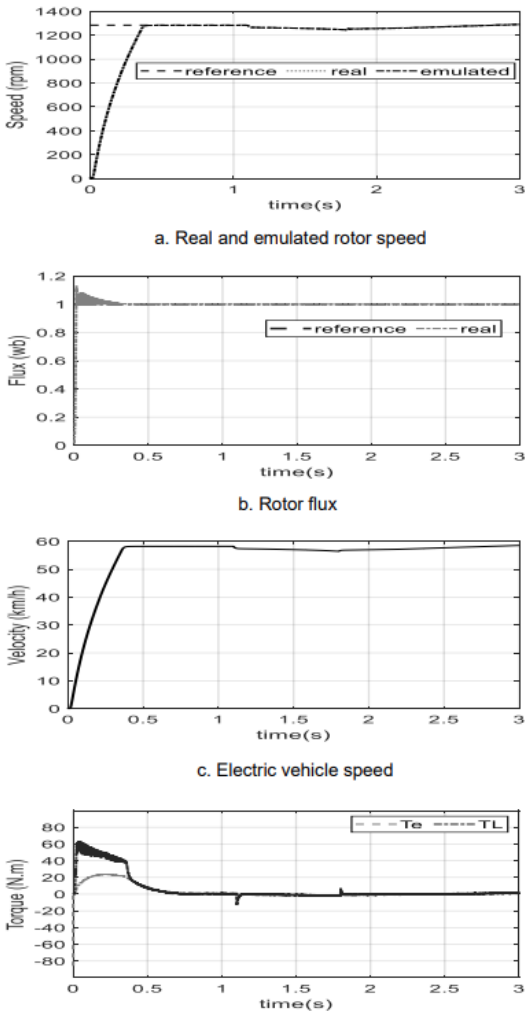

a. Real and emulated rotor speed

b. Rotor flux

c. Electric vehicle speed

Fig.12. Close up view of solar PV powered DTPIM based EV

As can be analyzed from current waveforms, it shows that it is nearly sinusoidal, the rotor flux and the electromagnetic torque track their references. So, the obtained results were very successful and confirm the validity of the proposed control. The speed of the DTPIM is decreased by decrease in irradiation level and speed is increased by increase in irradiation level.

Conclusion

This paper has proposed a solar photovoltaic (PV) fed DTPIM drive aimed at electric vehicle applications. From PV

system, the three- level boost converter is used here to step up the output voltage at the maximum power point level using the ANFIS because the MPPT algorithm based ANFIS performs its role correctly for the search of the maximum point of the power, where the point of maximum power moves to reach the new maximum point corresponding to this new insolation or temperature. Summing up the results, it can be concluded that this study show the feasibility of ANFIS approaches and the improved dynamic performance of the machine in the case of variations in weather conditions or load.

As a future work, we are looking forward to developing, implementing and testing our system.

***Authors**: Toufik Roubache, Department of Electrical Engineering, University of Msila, Algeria and Souad Chaouch, LSP-IE Laboratory, University of Batna2, Algeria, E-mail: toufik.roubache@gmail.com.*

REFERENCES

[1] Akca T., Ulu C., Obut S., ANFIS Based Inverse Controller Design for Liquid Level Control of a Spherical Tank, *Przegląd Elektrotechniczny,* 99 (2023), No. 2, 32-36.

[2] Fernando J.T.E., Anbal T., Induction motor downsizing as a low-cost strategy to save energy, Journal of Cleaner Production, 24(2012),117-131.

[3] Chakchouk W., Ben Regaya C., Zaafouri A., Sellami A., An improved fuzzy logic control of irrigation station, 4th International Conference on Control, Decision and Information Technologies (CoDIT), (2017), 259-264.

[4] Beghdadi A., Bentaallah A., Abden A., Optimization of Sliding Mode with MRAS Based Estimation for Speed Sensorless Control of DSIM Via GWO, *Przegląd Elektrotechniczny,* 97(2021), No. 6, 21-29.

[5] Villani M., Tursini M., Fabri G., Castellini L., High reliability permanent magnet brushless motor drive for aircraft application, IEEE Trans. Ind. Electron., 59(2012), No. 5, 2073-2081.

[6] Jin L., Norrga S., Zhang H., Wallmark O., Evaluation of a multiphase drive system in EV and HEV applications, In Proc. IEMDC.IEEE, (2015), 941-945.

[7] Chen Q., Liao C., Ouyang A., Li X., Xiao Q., Research and development of in-wheel motor driving technology for electric vehicles. Int. J. Electr. Hybrid Veh. 8(2016), 242-254.

[8] Sahraoui K., Katia K., Ameur A., A Robust Sensorless Iterated Extended Kalman Filter for Electromechanical Drive State Estimation, in EEA – Electrotehnica Electronica Automatica. 65(2017), No. 2, 46-53.

[9] Derbane A., Tabbache B., Ahriche A., A fuzzy logic approach based direct torque control and five-leg voltage source inverter for electric vehicle powertrains, Rev. Roum. Sci. Techn. – Électrotechn. Et Énerg, 66(2021), No. 1, 15-20.

[10] Belkacem S., Naceri F., Abdessemed R., Reduction of torque ripple in DTC for induction motor using input-output feedback linearization. Serbian Journal of Electrical Engineering, 8(2011), No.2, 97-110.

[11] Lazreg M., Bentaallah A., Input Output Linearization Control of Double Star Induction Machine, Rev. Roum. Sci. Techn. – Électrotechn. Et Énerg, 63(2018), No. 4, 423-428.

[12] De Castro R., Araujo R., Freitas D., Wheel slip control of EVs based on sliding mode technique with conditional integrators, IEEE Transaction on Industrial Electronics, 60(2013), No.8, 3256-3271.

[13] Nam K., Fujimoto H., Hori Y., Advanced motion control of electric vehicles based on robust lateral tire force control via active front steering, IEEE/ASME Transactions on Mechatronics, 19(2014), No. 1, 289-299.

[14] Yang Y., Liang Y., Xu G., Zhang J., Novel traction control of electric vehicle based on single wheel dynamics, Journal of Engineering, (2019), No. 23, 9006-9012.

[15] Hadjab M., Medjahed B., Comparison and statistical validation of a model of a photovoltaic module, International Journal of Energy, 6(2012), No. 4, 133-140.

[16] Jacomini R.V., Rocha C.M., Altuna J.A.T., Azcue J.L., Capovilla C.E., Squarezi A.J., Implementation of a Neuro-Fuzzy Direct Torque and Reactive Power Control for Doubly Fed Induction Motor, *Przegląd Elektrotechniczny,* 90 (2014), No. 10, 179-187.

[17] Gregor R., Rodas J., Speed Sensorless Control of Dual Three-Phase Induction Machine based on a Luenberger Observer for Rotor Current Estimation, 38th Annual Conference on IEEE Industrial Electronics Society, (2012), 3653-3658.

[18] Roubache T., Chaouch S., Nait said M., Sensorless Fault-Tolerant Control of an Induction Motor Based Electric Vehicle. J Electr Eng Technol, 11(2016), No. 5, 1423-1432.